Complex Energies and Transition-Dipoles for the Uracil anion Shape-type Resonances from stabilization curves via Padé

Gal Bouskila,[†] Arie Landau,[†] Idan Haritan,[†] Nimrod Moiseyev,[†,‡,¶] and Debarati Bhattacharya[*,†]

[†]*Schulich Faculty of Chemistry, Technion-Israel Institute of Technology, Haifa, 3200003, Israel*

[‡]*Department of Physics, Technion-Israel Institute of Technology, Haifa, 32000, Israel*

[¶]*Russell-Berrie Nanotechnology Institute, Technion-Israel Institute of Technology, Haifa 32000, Israel*

E-mail: debarati@campus.technion.ac.il

Abstract

Absorption of slow moving electrons by neutral ground state nucleobases have been known to produce resonances metastable states. There are indications that such metastable states may play a key-role in DNA/RNA damage. Therefore, herein, we present an *ab-initio* non-Hermitian investigation of the resonance positions and decay rates for the low lying shape-type states of the uracil anion. In addition, we calculate the complex transition dipoles between these resonance states. We employ the resonance via Padé (RVP) method to calculate these complex properties from real stabilization curves by analytical dilation into the complex plane. This method has already been successfully applied to many small molecular systems and herein we present the first application of RVP to a medium-size system. The presented resonance energies are converged with respect to the size of the basis set and compared with previous theoretical works and experimental findings. Complex transition dipoles between the shape-type resonances are computed using the energy-converged basis set. The ability to calculate *ab-initio* energies and lifetimes of biologically relevant systems opens the door for studying reactions of such systems in which autoionization takes place. While the ability to also calculate their complex transition dipoles open the door for studying photo induced dynamics of such biological molecules.

Introduction

High energy particles may lead to DNA damage in the form of single and double strand break. This kind of damage can be extremely dangerous, as it is considered genotoxic, mutagenic and recombinogenic.[1] Apparently, those processes are not produced by the primary high-energy quanta, but by secondary species such as free electrons with low energy.[2] In practice, due to the radiation, a large quantity of low energy electrons (LEE) with an energy distribution lying below 10 eV is produced; these electrons are likely to induce significant amount of chemical damage within the cell.[3–6] LEE attached to molecules often lead to anions in a metastable state, resonances. A resonance is a metastable state of the system, in which the system does not break into subsystems, even though it has enough energy to do so. Instead, the break up process requires some finite time (decay rate). In non-Hermitian quantum mechanics resonances are associated with complex eigenvalues: $E = E_r - \frac{i}{2}\Gamma$, where the real part relates to the energy *position* of the resonance, while the imaginary part relates to the *decay* rate (lifetime/width) of the metastable state.[7]

Anionic resonances in biological molecules, like DNA and RNA nucleobases, may lead to dissociative electron attachment (DEA). The outcome of DEA process highly depends on the energy and lifetime of the attached electron, i.e., it determines fragmentation or non-dissociative relaxation mechanism.[8–10] To get a better understanding of the mechanisms responsible for DNA damage by LEE via DEA, we need to acquire more knowledge on the interaction of LEE with nucleobases.[11] Studying the mechanism causing DNA damage has been of great interest in the experimental and theoretical science communities, however, showing various processes with very different energy values.[12–18] Therefore, an *ab-initio* treatment is needed. Such a treatment can help to explain the interaction of resonances with light (as it is necessary to calculate complex transition dipole in order to understand such interaction).

Recently we introduced and benchmarked a new method known as resonance via Padé (RVP). This method use the stabilization technique ,[19–21] to calculate atomic and molecular resonances from standard (Hermitian) electronic structure packages.[22,23] So far, the method had been successfully applied to small molecular and atomic systems such as, He^{*},[22,23] H_2^{*},[22,23] H^{*-},[22] N_2^{-},[23]and Be^{*},.[24] Moreover, RVP was even used to calculate the $He^{*}-H_2$ complex potential energy surfaces (CPESs) in order to interpret and describe cold molecular collision experiments,[25–27] these CPESs were used to compute theoretical cross sections that were in remarkable agreement with the measurements.[28,29] Additionally, RVP was also used for predicting the interatomic Coulombic decay (ICD) products within the extreme Li–He system.[30,31]

In light of the above, it is of great interest in treating large chemical system. Therefore, in this work, we present the first application of RVP to a medium-size system, the uracil anion (with 59 electrons), while focusing on its shape-type resonances.

Uracil is the smallest nucleobase in RNA and it resembles the DNA nucleobase thymine, making it appealing for theoretical calculations. The anionic resonance states of uracil are formed by the attachment of an electron to one of the unoccupied virtual (π^{*} and σ^{*}) orbitals of the neutral ground state. The π^{*} shape-type resonance have been observed experimentally and calculated theoretically, while the σ^{*} have only been treated theoretically .[32,33] Many theoretical studies on uracil can be found in the literature. Earlier works on the uracil anion present a large range of results, including the stabilized Koopmans' theorem (S-KT) stabilization,[34] stabilized Koopmans-based approximation (S-KB) stabilization,[34] R-matrix,[35,36] Schwinger multichannel method with pseudopotential (SMCPP).[37] However, the most recent studies include the Generalized Padé Approximation (GPA)/stabilization graphs approach,[38] and complex absorbing potential (CAP)/symmetry-adapted cluster-configuration interaction (SAC-CI) approach.[39] Herein, we compare these results with ours. In particular, it is interesting to compare RVP with GPA. While both of these methods are based on stabilization graphs, they are essentially different, and it was shown by Haritan and Moiseyev that each method has its' own advantages and disadvantages.[40] Nevertheless, RVP possess several clear advantages: the RVP fitting is less sensitive than the GPA fitting to the chosen data set[40] and the RVP allows calculations of other complex properties, such as the complex transition dipoles,[41] which are essential for studying light-matter interactions. In fact, herein we report the transition dipoles between the resonance states. This data can be used, for example, to calculate the photoionization spectra and the Fano asymmetry parameter.[42] Thus, the information presented in this work enables future investigation of uracil and the mechanisms involving DEA.

In the last section of this work, we will shortly discuss a mechanism that may minimize radiation damage to biological systems, such as uracil, and illustrates the need for calculating complex energies as well as transition dipoles.

Computational Details

The neutral geometry of uracil is optimized at the MP2/cc-pVTZ level of theory with a Cs symmetry (see Supporting Information for more details).[43,44] The energy positions and decay rates of the three lowest π^* shape-type resonances of the uracil anion are calculated using the RVP technique. Equation-of-motion coupled-cluster with singles and doubles for electron affinities (EOM-EA-CCSD)[45] is used to calculate the stabilization graphs, where the singlet ground state of the neutral uracil serves as the reference state. All calculations were performed with the quantum chemistry package Q-Chem.[46]

We perform a basis set convergence employing the following basis sets: Pople's 6-31+G, 6-311+G, and 6-311+G(2d,p), as well as Dunning's aug-cc-pVDZ, aug-cc-pVDZ+1s1p1d (in which we add one diffuse function of s, p and d angular momentum on each atom except for the hydrogen atoms) and aug-cc-pVTZ. Moreover, upon concluding that a triple-ζ basis set is essential, we investigate the effect of adding diffuse functions systematically on top of the cc-pVTZ basis set (while using aug-cc-pVTZ for the hydrogen atoms). We report six such cc-pVTZ sets, which are augmented with +1s1p, +2s2p, +3s3p, +2s2p1d, +3s2p1d and +2s2p2d. These additional diffuse functions were added in an even-tempered fashion (with respect to the value of the original most diffuse function with an even-temper parameter of

2). All the employed basis sets are presented in the Supporting Information (SI).

The stabilization graphs are obtained via partial scaling,[24] i.e., only the exponents of the most diffuse functions are divided by a real scaling parameter (α). The range of the scaling parameter α varies between 0.4 and 3.0. For the cc-pVTZ+XsYpZd basis sets we scale all the additional +XsYpZd diffuse functions (where for hydrogen we scale the most diffuse s, p and d functions). For aug-cc-pVXZ (X=D or T) we scale the most diffuse s, p and d functions, whereas for aug-cc-pVDZ+1s1p1d we scale also the added +1s1p1d functions. For 6-31+G we scale the two most diffuse s and p functions (where for hydrogen only the s), for 6-311+G two s and two p functions (for hydrogen two s), and for 6-311+G(2d,p) two s, two p and one d (where for hydrogen one s and one p).

Within the RVP method a Padé function is dilated into the complex plane based on data obtained from real stabilization calculation. The data is taken from the stable (analytic) region of a branch, however several such branches may exist. The reported complex energies correspond to the statistically best-behaved results, see the Method Section for additional details. Fig. 1 presents such a stabilization graph (additional graphs, using different basis sets, are given in the SI). Fig. 1a presents the entire spectrum, whereas Figs. 1b, c and d focuses on the stable region associated with each electronic state. These regions are marked with circles. The stable regions in Figs. 1b, c and d provide the best results from a statistical point of view. However, for calculating transition dipoles, we require the energy stable-regions of the relevant states to overlap. Therefore we chose a different branch for calculating the transition dipoles (Fig. 2a) than for the energy calculations (Fig. 1c))

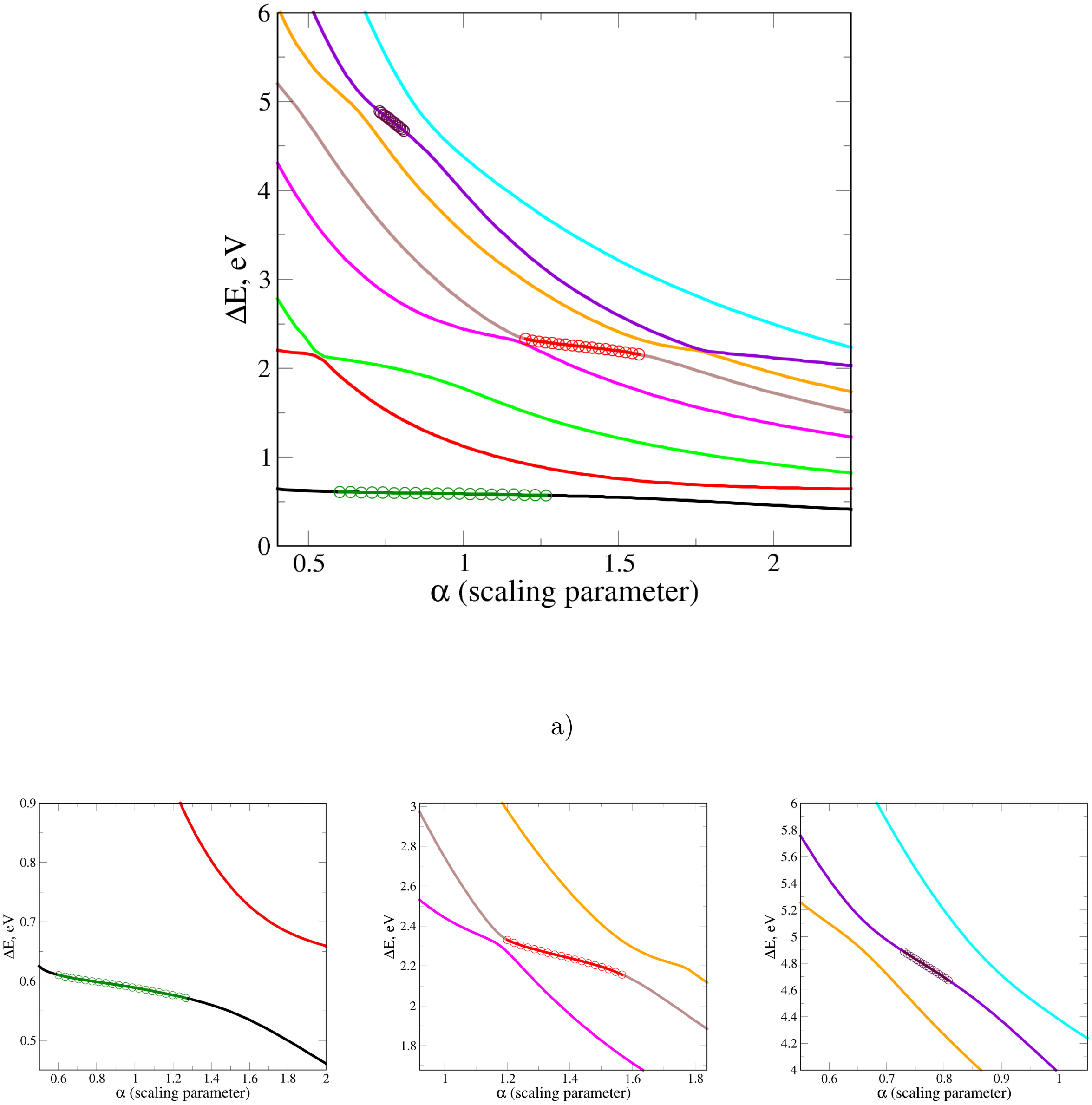

a)

b)

c)

d)

Figure 1: (a) Energy stabilization plot of the uracil anion at the EOM-EA-CCSD/cc-pVTZ+2s2p2d (H: aug-cc-pVTZ) level. The circles represent the sets of points used as inputs for the RVP method (i.e. the stable region). Zoom in: (b) $1\pi^*$, (c) $2\pi^*$ and (d) $3\pi^*$.

Results and Discussions

Complex Energies – Convergence with respect to the size of the one-electron basis set

The computed complex energies (positions and widths) of the three lowest-lying shape type resonances of the uracil anion are presented in Table 1. In this table, we examine the the convergence of the results with respect to the size of the basis set, where special attention is given to the role of the diffuse functions. The results are sub-divided into four panels. In the first panel, we use different Pople's basis sets. A comparison between the bases in this panel clearly highlights the importance of using a triple-ζ (TZ) basis set: The resonance energy position for all three shape-type resonances decreases on going from the 6-31+G to the 6-311+G basis sets, whereas the effect of additional polarization functions [6-311+G(2d,p)] is even more pronounced.

Table 1: Energy positions (E_r) and widths (Γ, in parenthesis) of the uracil anion using the RVP method with electronic calculation at the EOM-EA-CCSD level using different basis sets (the total number of basis functions is indicated in parenthesis).

		$E_r(\Gamma)$, eV	
Basis sets	$1\pi^*$	$2\pi^*$	$3\pi^*$
6-31+G (112)	1.173 (0.015)	2.928 (0.068)	6.108 (0.210)
6-311+G (148)	1.103 (0.042)	2.795 (0.089)	5.889 (0.204)
6-311+G(2d,p) (240)	0.748 (0.012)	2.556 (0.072)	5.646 (0.182)
aug-cc-pVDZ (220)	0.761 (0.019)	2.486 (0.094)	5.490 (0.404)
aug-cc-pVDZ+1s1p1d (292)	0.738 (0.014)	2.440 (0.170)	5.277 (0.673)
aug-cc-pVTZ (460)	0.582 (0.011)	2.240 (0.115)	4.929 (0.339)
cc-pVTZ+1s1p† (364)	0.638 (0.002)	2.204 (0.084)	4.931 (0.635)
cc-pVTZ+2s2p† (396)	0.617 (0.006)	2.321 (0.182)	5.024 (0.649)
cc-pVTZ+3s3p† (428)	0.610 (0.008)	2.333 (0.126)	5.078 (0.677)
cc-pVTZ+2s2p1d† (436)	0.602 (0.010)	2.252 (0.177)	5.016 (0.661)
cc-pVTZ+3s2p1d† (444)	0.598 (0.012)	2.245 (0.176)	4.998 (0.660)
cc-pVTZ+2s2p2d† (476)	0.597 (0.014)	2.183 (0.140)	4.858 (0.657)

† with aug-cc-pVTZ for the hydrogens

The importance of the polarized functions in Pople's basis sets naturally led us to check highly polarised Dunning's basis sets. Therefore, in the second panel, we compare Dunning's correlation-consistent augmented-DZ and TZ basis sets. We observe that at the double ζ level (aug-cc-pVDZ), we obtain very similar results to the largest Pople basis set. Yet, the decay rate for the $3\pi^*$ resonance state had an abrupt increase to $\sim$0.4 eV as compared to $\sim$0.2 eV in Pople's basis sets. Additional diffuse basis functions play a key role evaluating of the widths (-2ImE) as can be seen from comparing the aug-cc-pVDZ results with aug-cc-pVDZ+1s1p1d results. Furthermore, on going from aug-cc-pVDZ to aug-cc-pVTZ the energy positions (Re$E = E_r$) are clearly affected. Therefore, in the third panel we employ the cc-pVTZ basis set and systematically augment it with increasing number of diffuse functions.

Notice that the energy position differences in the 3^{rd} panel, are within 0.1 eV, thus the energy position is converged with respect to the additional diffuse basis functions. As for the width, we see in the 3^{rd} panel that adding only +1s1p basis functions is not sufficient and that adding +2s2p is essential. On the other hand, we see that while adding +3s3p basis functions makes an effect (on the $2\pi^*$ width), this effect is small. Therefore, in the 4^{th} panel we examine the effect of adding d-functions on top of the +2s2p diffuse functions as was used in the 3^{rd} panel. Clearly, adding only one d-type function (+2s2p vs. +2s2p1d) and augmenting via +3s2p1d has a very small effect on the results. However, adding two *d*-diffuse functions (+2s2p vs. +2s2p2d) has a pronounced effect on the results. Therefore, we conclude that the largest cc-pVTZ+2s2p2d is the optimal basis set.

Table 2 presents our converged results in comparison with the most recent theoretical results and with the experimental energy positions (no widths are available). The theoretical results are showing the same trend. On the contrary, they clearly overestimate the experimental energy positions. However, the agreement between the different theoretical values is encouraging, in particular when considering the large range of results in earlier studies.[34–37]

Table 2: Comparison of the energy positions (E_r) and widths (Γ, in parenthesis) of the lowest three shape-type resonances of uracil anion using RVP (present work) with other theoretical methods and experimental results.

	$E_r(\Gamma)$, eV		
	$1\pi^*$	$2\pi^*$	$3\pi^*$
RVP†	0.5970 (0.014)	2.1833 (0.140)	4.8579 (0.657)
GPA*	0.61 (0.02)	2.28 (0.07)	4.98 (0.34)
CAP**	0.57 (0.05)	2.21 (0.10)	4.82 (0.58)
Exp.[47]	0.22	1.58	3.83

† this work, EOM-EA-CCSD/cc-pVTZ+2s2p2d (H: aug-cc-pVTZ)

* EOM-EA-CCSD/aug-cc-pVDZ+1s1p1d[48,49]

** SAC-CI/cc-pVDZ+[2s5p2d][50]

Complex Transition Dipoles for the Uracil Anion Resonances

Using the converged basis set, cc-pVTZ+2s2p2d, we also calculated the complex transition dipoles between the three resonance states of the uracil anion. Employing the RVP technique to compute complex transition dipoles have been successfully benchmarked in Ref 41. Herein, we present the first application of RVP to property calculation of a medium-size molecular system of a biological interest. The complex transition dipoles are an essential in order to study light-matter interactions within the non-Hermitian formalism.

Figure 2 illustrates the RVP procedure for calculating complex transition dipoles for the $1\pi^* \leftrightarrow 2\pi^*$ case, i.e., between the first and second shape resonance states. Figure 2a depicts the energy stabilisation plot for these shape-type states. The overlap between the two stable regions is highlighted in black. This energy overlap area, in parameter space, corresponds to a "macroscopic stability" in the transition dipole plot (an analytic area in which the change in the values is relatively small, in the current case less than 12%). The concept of "macroscopic stability" was defined for cases where the variational principle does not hold.[51] In those cases the behaviour of the continuum states, when scaled by a parameter, is not well defined, unlike in the energy stabilization case. In the standard energy stabilization graphs the energy of a continuum state will always decrease as the real scaling parameter α increases, i.e., as the space spanned by the basis set is increased. As a result, in the dipole

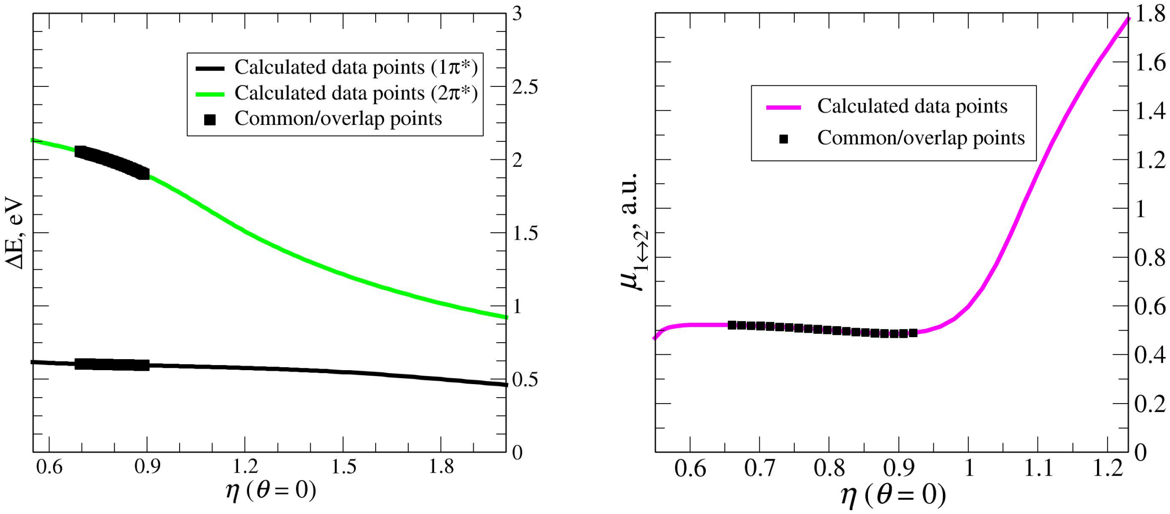

a) b)

Figure 2: (a) Energy stabilization plot for uracil anion, at the EOM-EA-CCSD/cc-pVTZ+2s2p2d (H: aug-cc-pVTZ) level. The black squares represent the sets of data points that are common between the two stabilised areas (the overlap). (b) Transition dipole stabilisation plot for $1\pi^* \leftrightarrow 2\pi^*$. The black data points corresponds to a macroscopic stable part on the plot, which has the same α-range as the overlap area in the energy graph. These points are taken as inputs for the analytical dilation in the Padé approximate.

case we may obtain different shapes of stabilization graphs, see Figure 2b and Figs. 13 and 14 in the SI. The complex transition dipoles are calculated in a similar manner to the procedure for the complex energies. The data points marked in black in Figure 2b serve as input points for the Padé fitting. This is followed by analytically dilation of the Padé function into the complex plane and search for clusters of stationary points, which corresponds to the complex dipoles. The outcome of this procedure, i.e., the complex transition dipoles between the three resonance states, are given in Table 3. The real part dominant the three transition dipoles, where the imaginary part corresponds to about 1% of it or less.

Table 3: Complex transition dipole moments, real and imaginary parts (in a.u.) between the three lowest shape-type resonances of uracil anion obtained in this work using RVP. Basis set: cc-pVTZ+2s2p2d

Reμ	Imμ	Reμ	Imμ	Reμ	Imμ
$1\pi^* \leftrightarrow 2\pi^*$		$1\pi^* \leftrightarrow 3\pi^*$		$2\pi^* \leftrightarrow 3\pi^*$	
5.089e-01	-3.599e-03	8.782e-01	-6.017e-03	8.204e-01	-1.628e-02

A simple example that illustrates the need for complex transition dipoles is the research on minimizing DNA damage via dissociative electron attachment. According to Matsika and coworkers the $3\pi^*$ state, unlike the $1\pi^*$ and the $2\pi^*$ states, is reactive with respect to CO elimination.[10] Therefore it is desirable to study the elimination of electron attachment to the $3\pi^*$ state, i.e., we wish to study the transition of the electron from $3\pi^*$ to the $1\pi^*$ or $2\pi^*$ states. This study is only possible if one has the transition dipole between the states. Hence, this data is extremely important for future works. However, simply using a laser to induce a transition from one resonance to another dose not solve the problem. Since a typical laser pulse is of low intensity and their envelop supports many optical cycles, the oscillations between the two resonances are unavoidable. Nevertheless, by using chirped laser pulses an asymmetric switch can be obtained, which enables the transfer of $3\pi^*$ to $2\pi^*$ or $1\pi^*$ without the backward transfer to $3\pi^*$. The asymmetric switch is obtained as the laser encircles a special point in the frequency-intensity 2D space. The special point, know as an exceptional point, is a point in this 2D space in which two resonances coalesce (i.e non-Hermitian degeneracy).[7] Explaining this mechanism is out of the scope of this work, for a general theoretical representation see Ref 52 and for an experimental demonstration of such an asymmetric switch see Ref 53. Notwithstanding, we perceive that in order to design an asymmetric switch one requires the complex energies (Table 2) and transition dipoles (Table 3).

Summary

We study the three lowest shape-type resonances of the uracil anion using the resonance via Padé (RVP) approach. RVP was already successfully used in studying atomic and small molecular resonances, and herein we apply this approach to a medium-size chemical system with a biological interest. The presented results are converged with respect to the one-electron basis set and compared to other theoretical and experimental values. In this work we have shown the key role of polarized and diffuse basis functions (up to d-functions) in the calculation of uracil anion resonances, resulting with cc-pVTZ+2s2p2d as our optimal basis set. In addition, we present the calculated complex transition dipoles between the different resonance states. These properties are essential in studying light-matter interaction within the uracil anion, which may lead to progress in understanding the mechanism and even minimize DNA/RNA damage.

Methods

The resonances energies are calculated with the RVP method. This method uses Hermitian electronic structure calculations and anaytically continues it into the Non-Hermitian regime via the Padé approximant. In practice, the method uses the stable part of the stabilization graph as input, and produces as an output the relevant complex energy of the corresponding resonance.

In this study, we started by generating the stabilization graphs, using standard Hermitian electronic structure formalism.[19–21] To generate such graphs, we scaled a finite Gaussian basis set by a real factor (α), i.e., we divided the exponent of the most diffuse basis functions by α. For $\alpha < 1$ the space spanned by the basis set compresses and for $\alpha > 1$ it expands. The plot of the eigenvalues (energies) as function of the α is known as a stabilization graph. Continuum, resonance and bound states behave differently upon scaling due to the different nature of their associated wave-functions. The continuum states are associated with a delocalized wave-function, whereas the bound states are localized in the interaction region and the resonance states are partially localized.[7] Consequently, bound eigenvalues would not depend on the scaling parameter and the resonance eigenvalues will have small dependency on the scaling parameter. Contrary, continuum eigenvalues will strongly depend on the scaling factor. For the resonance eigenvalues, unlike for the bound ones, we expect crossing attempts by continuum eigenvalues, also known as, avoided crossings. This behaviour of the resonance states translated to stable region in the stabilization graphs, which is know to be an analytic region.[22,40,54]

To calculate the resonances position as well as its decay rate, we used analytical continuation of the real data (stabilization graphs) to the complex plane. In practice, we used the Padé approximant (the Schlessinger point method[54]) to fit the stable part of the stabilization graph two polynomials:

$$E(\alpha) = \frac{P(\alpha)}{Q(\alpha)}. \tag{1}$$

Next, we substituted a complex parameter $\eta = \alpha e^{i\theta}$ into the fitted energy function and the resonances are identified as stationary points (SPs) in the complex plane, i.e., they satisfy:

$$\frac{\partial E(\eta)}{\partial \eta}\Big|_{\eta^{SP}} = 0 \tag{2}$$

Graphically, these stationary points are associated with cusps in the α-and θ-trajectories. A θ-trajectory is generated by fixing α and varying θ over a range of values, the opposite is true for the α trajectory. Convergence is achieved when those two trajectories from cusps that meet.[55] Finally, we checked the stability of the complex resonance energies with respect to small modifications of the Padé input data set using a statistical approach.[23] We choose many input data sets for the Padé fitting and we are looking for clusters in the complex energy space, these clusters are associated with resonance plotted as a function the Padé input. That is, the average of the clusters with the smallest deviation is the reported result. Notice that those chosen data sets successfully reproduced the original stabilization curve; we consider this as a numerical proof for the analiticity of the selected stable region.[22,56]

Data Availability Statement

The data that support the findings of this study are available from the corresponding author upon reasonable request.

Acknowledgement

This research was supported by the I-Core: the Israeli Excellence Centre ”Circle of light”, by the Israel Science Foundation Grant No. 1661/19. I.H. acknowledge the support of the Azrieli foundation.

Supporting Information Available

The employed basis sets and the associated stabilization graphs for the energy and transition dipoles are presented in the SI.

References

(1) Lipton, M. S.; Fuciarelli, A. F.; Springer, D. L.; Edmonds, C. G. *Radiation damage in DNA: Structure/function relationships at early times*; 1995.

(2) von Sonntag, C., et al. *The chemical basis of radiation biology*; Taylor & Francis London, 1987.

(3) LaVerne, J. A.; Pimblott, S. M. Electron energy-loss distributions in solid, dry DNA. *Radiation Research* **1995**, *141*, 208–215.

(4) Uehara, S.; Nikjoo, H.; Goodhead, D. T. Comparison and assessment of electron cross sections for Monte Carlo track structure codes. *Radiation Research* **1999**, *152*, 202–213.

(5) Cobut, V.; Frongillo, Y.; Patau, J.; Goulet, T.; Fraser, M.; Jay-Gerin, J. Monte Carlo simulation of fast electron and proton tracks in liquid water-I. Physical and physicochemical aspects. *Radiation Physics and Chemistry* **1998**, *51*, 229–244.

(6) Srdoč, D. Average Energy Required To Produce An Ion Pair, ICRU Report 31. Published by the International Commission on Radiation Units and Measurements. Washington, DC, USA. 1981.

(7) Moiseyev, N. *Non-Hermitian quantum mechanics*; Cambridge University Press, Cambridge, 2011.

(8) Kawarai, Y.; Weber, T.; Azuma, Y.; Winstead, C.; McKoy, V.; Belkacem, A.; Slaughter, D. Dynamics of the dissociating uracil anion following resonant electron attachment. *The Journal of Physical Chemistry Letters* **2014**, *5*, 3854–3858.

(9) Zhou, C.; Matsika, S.; Kotur, M.; Weinacht, T. C. Fragmentation pathways in the uracil radical cation. *The Journal of Physical Chemistry A* **2012**, *116*, 9217–9227.

(10) Fennimore, M. A.; Karsili, T. N.; Matsika, S. Mechanisms of H and CO loss from the uracil nucleobase following low energy electron irradiation. *Physical Chemistry Chemical Physics* **2017**, *19*, 17233–17241.

(11) Sanche, L. Nanoscopic aspects of radiobiological damage: Fragmentation induced by secondary low-energy electrons. *Mass Spectrometry Reviews* **2002**, *21*, 349–369.

(12) Huels, M. A.; Boudaïffa, B.; Cloutier, P.; Hunting, D.; Sanche, L. Single, double, and multiple double strand breaks induced in DNA by 3- 100 eV electrons. *Journal of the American Chemical Society* **2003**, *125*, 4467–4477.

(13) Pan, X.; Cloutier, P.; Hunting, D.; Sanche, L. Dissociative electron attachment to DNA. *Physical Review Letters* **2003**, *90*, 208102.

(14) Sanche, L. Interactions of low-energy electrons with atomic and molecular solids. *Scanning Microscopy* **1995**, *9*, 1.

(15) Charlton, D.; Humm, J. A method of calculating initial DNA strand breakage following the decay of incorporated 125I. *International Journal of Radiation Biology* **1988**, *53*, 353–365.

(16) Nikjoo, H.; Martin, R. F.; Charlton, D. E.; Terrissol, M.; Kandaiya, S.; Lobachevsky, P. Modelling of Auger-induced DNA damage by incorporated125I. *Acta Oncologica* **1996**, *35*, 849–856.

(17) Prise, K. M.; Folkard, M.; Michael, B. D.; Vojnovic, B.; Brocklehurst, B.; Hopkirk, A.; Munro, I. H. Critical energies for SSB and DSB induction in plasmid DNA by low-energy photons: action spectra for strand-break induction in plasmid DNA irradiated in vacuum. *International Journal of Radiation Biology* **2000**, *76*, 881–890.

(18) Hanel, G.; Gstir, B.; Denifl, S.; Scheier, P.; Probst, M.; Farizon, B.; Farizon, M.;

Illenberger, E.; Märk, T. Electron attachment to uracil: Effective destruction at subexcitation energies. *Physical Review Letters* **2003**, *90*, 188104.

(19) Holeien, E. 141. E. Holeien and J. Midtal. *J. Chem. Phys* **1966**, *45*, 2209.

(20) Hazi, A. U.; Taylor, H. S. Stabilization method of calculating resonance energies: model problem. *Physical Review A* **1970**, *1*, 1109.

(21) Landau, A. Shaping and controlling stabilisation graphs for calculating stable complex resonance energies. *Molecular Physics* **2019**, *117*, 2029–2042.

(22) Landau, A.; Haritan, I.; Kapralova-Zd'anska, P. R.; Moiseyev, N. Atomic and molecular complex resonances from real eigenvalues using standard (hermitian) electronic structure calculations. *The Journal of Physical Chemistry A* **2016**, *120*, 3098–3108.

(23) Landau, A.; Haritan, I. The Clusterization Technique: A Systematic Search for the Resonance Energies Obtained via Padé. *The Journal of Physical Chemistry A* **2019**, *123*, 5091–5105.

(24) Ben-Asher, A.; Landau, A.; Moiseyev, N. Uniform vs Partial Scaling within Resonances via Pade Based on the Similarities to Other Non-Hermitian Methods: Illustration for the Beryllium 1 s 22 p 3 s State. *Journal of Chemical Theory and Computation* **2021**, *17*, 3435–3444.

(25) Narevicius, E.; Raizen, M. G. Toward cold chemistry with magnetically decelerated supersonic beams. *Chemical Reviews* **2012**, *112*, 4879–4889.

(26) Lavert-Ofir, E.; Shagam, Y.; Henson, A. B.; Gersten, S.; Kłos, J.; Żuchowski, P. S.; Narevicius, J.; Narevicius, E. Observation of the isotope effect in sub-kelvin reactions. *Nature Chemistry* **2014**, *6*, 332–335.

(27) Shagam, Y.; Klein, A.; Skomorowski, W.; Yun, R.; Averbukh, V.; Koch, C. P.; Narevicius, E. Molecular hydrogen interacts more strongly when rotationally excited at low temperatures leading to faster reactions. *Nature Chemistry* **2015**, *7*, 921–926.

(28) Bhattacharya, D.; Ben-Asher, A.; Haritan, I.; Pawlak, M.; Landau, A.; Moiseyev, N. Polyatomic ab initio complex potential energy surfaces: Illustration of ultracold collisions. *Journal of Chemical Theory and Computation* **2017**, *13*, 1682–1690.

(29) Bhattacharya, D.; Pawlak, M.; Ben-Asher, A.; Landau, A.; Haritan, I.; Narevicius, E.; Moiseyev, N. Quantum effects in cold molecular collisions from spatial polarization of electronic wave function. *The Journal of Physical Chemistry Letters* **2019**, *10*, 855–863.

(30) Landau, A.; Ben-Asher, A.; Gokhberg, K.; Cederbaum, L. S.; Moiseyev, N. Ab initio complex potential energy curves of the He*(1 s 2 p 1P)–Li dimer. *The Journal of Chemical Physics* **2020**, *152*, 184303.

(31) Ben-Asher, A.; Landau, A.; Cederbaum, L. S.; Moiseyev, N. Quantum Effects Dominating the Interatomic Coulombic Decay of an Extreme System. *The Journal of Physical Chemistry Letters* **2020**, *11*, 6600–6605.

(32) Gonzalez-Ramirez, I.; Segarra-Marti, J.; Serrano-Andres, L.; Merchan, M.; Rubio, M.; Roca-Sanjuan, D. On the N1–H and N3–H Bond dissociation in uracil by low energy electrons: a CASSCF/CASPT2 study. *Journal of Chemical Theory and Computation* **2012**, *8*, 2769–2776.

(33) Sommerfeld, T. Intramolecular electron transfer from dipole-bound to valence orbitals: Uracil and 5-chlorouracil. *The Journal of Physical Chemistry A* **2004**, *108*, 9150–9154.

(34) Cheng, H.-Y.; Chen, C.-W. Energy and lifetime of temporary anion states of uracil by stabilization method. *The Journal of Physical Chemistry A* **2011**, *115*, 10113–10121.

(35) Dora, A.; Tennyson, J.; Bryjko, L.; van Mourik, T. R-matrix calculation of low-energy electron collisions with uracil. *The Journal of Chemical Physics* **2009**, *130*, 164307.

(36) Gianturco, F.; Lucchese, R. Radiation damage of biosystems mediated by secondary electrons: Resonant precursors for uracil molecules. *The Journal of Chemical Physics* **2004**, *120*, 7446–7455.

(37) Kossoski, F.; Bettega, M.; Varella, M. d. N. Shape resonance spectra of uracil, 5-fluorouracil, and 5-chlorouracil. *The Journal of chemical physics* **2014**, *140*, 024317.

(38) Thodika, M.; Fennimore, M.; Karsili, T. N.; Matsika, S. Comparative study of methodologies for calculating metastable states of small to medium-sized molecules. *The Journal of Chemical Physics* **2019**, *151*, 244104.

(39) Kanazawa, Y.; Ehara, M.; Sommerfeld, T. Low-lying π^* resonances of standard and rare DNA and RNA bases studied by the projected CAP/SAC–CI method. *The Journal of Physical Chemistry A* **2016**, *120*, 1545–1553.

(40) Haritan, I.; Moiseyev, N. On the calculation of resonances by analytic continuation of eigenvalues from the stabilization graph. *The Journal of Chemical Physics* **2017**, *147*, 014101.

(41) Bhattacharya, D.; Landau, A.; Moiseyev, N. Ab Initio Complex Transition Dipoles between Autoionizing Resonance States from Real Stabilization Graphs. *The Journal of Physical Chemistry Letters* **2020**, *11*, 5601–5609.

(42) Pick, A.; Kaprálová-Žďánská, P. R.; Moiseyev, N. Ab-initio theory of photoionization via resonances. *The Journal of Chemical Physics* **2019**, *150*, 204111.

(43) Møller, C.; Plesset, M. S. Note on an approximation treatment for many-electron systems. *Physical review* **1934**, *46*, 618.

(44) Dunning Jr, T. H. Gaussian basis sets for use in correlated molecular calculations. I. The atoms boron through neon and hydrogen. *The Journal of chemical physics* **1989**, *90*, 1007–1023.

(45) Krylov, A. I. Equation-of-motion coupled-cluster methods for open-shell and electronically excited species: The hitchhiker's guide to Fock space. *Annu. Rev. Phys. Chem.* **2008**, *59*, 433–462.

(46) Epifanovsky, E.; Gilbert, A. T.; Feng, X.; Lee, J.; Mao, Y.; Mardirossian, N.; Pokhilko, P.; White, A. F.; Coons, M. P.; Dempwolff, A. L., et al. Software for the frontiers of quantum chemistry: An overview of developments in the Q-Chem 5 package. *The Journal of Chemical Physics* **2021**, *155*, 084801.

(47) Aflatooni, K.; Gallup, G. A.; Burrow, P. Electron attachment energies of the DNA bases. *The Journal of Physical Chemistry A* **1998**, *102*, 6205–6207.

(48) Fennimore, M. A.; Matsika, S. Core-excited and shape resonances of uracil. *Physical Chemistry Chemical Physics* **2016**, *18*, 30536–30545.

(49) Fennimore, M. A.; Matsika, S. Correction: Core-excited and shape resonances of uracil. *Physical Chemistry Chemical Physics* **2017**, *19*, 29005–29006.

(50) Ehara, M.; Kanazawa, Y.; Sommerfeld, T. Low-lying π resonances associated with cyano groups: A CAP/SAC-CI study. *Chemical Physics* **2017**, *482*, 169–177.

(51) Moiseyev, N.; Weinhold, F. Criteria of accuracy of resonance eigenvalues. *International Journal of Quantum Chemistry* **1980**, *17*, 1201–1211.

(52) Uzdin, R.; Mailybaev, A.; Moiseyev, N. On the observability and asymmetry of adiabatic state flips generated by exceptional points. *Journal of Physics A: Mathematical and Theoretical* **2011**, *44*, 435302.

(53) Doppler, J.; Mailybaev, A. A.; Böhm, J.; Kuhl, U.; Girschik, A.; Libisch, F.; Milburn, T. J.; Rabl, P.; Moiseyev, N.; Rotter, S. Dynamically encircling an exceptional point for asymmetric mode switching. *Nature* **2016**, *537*, 76–79.

(54) Schlessinger, L. Use of analyticity in the calculation of nonrelativistic scattering amplitudes. *Physical Review* **1968**, *167*, 1411.

(55) Moiseyev, N.; Friedland, S.; Certain, P. R. Cusps, θ trajectories, and the complex virial theorem. *The Journal of Chemical Physics* **1981**, *74*, 4739–4740.

(56) Landau, A.; Bhattacharya, D.; Haritan, I.; Ben-Asher, A.; Moiseyev, N. Ab initio complex potential energy surfaces from standard quantum chemistry packages. *Advances in Quantum Chemistry* **2017**, *74*, 321–346.